ChemElectroChem

Research Article
doi.org/10.1002/celc.202400020

Chemistry Europe
European Chemical Societies Publishing

www.chemelectrochem.org

An Analysis of Calendaric Aging over 5 Years of Ni-Rich 18650-Cells with Si/C Anodes

Fabian Frie,*[a, b] Heinrich Ditler,[a, b] Sebastian Klick,[a, b] Gereon Stahl,[a, b] Christiane Rahe,[a, b] Tala Ghaddar,[a, b] and Dirk Uwe Sauer[a, b, c, d, e]

Calendaric lifetime testing of lithium-ion cells is time-consuming and resource-intensive. As Dubarry et al.[1] state, testing is often limited to a few aging conditions. This paper presents the results of a long-term aging study on lithium-ion cells with a nickel-rich NCA cathode and a graphite-silicon anode. 69 cells were stored at 5 different voltages and under 4 different temperatures for 5 years. Regular reference performance tests (RPT) provide insights for State of Health (SoH) calculation and further analysis through differential voltage analysis. The results are verified against post-mortem analyses. The long aging period enables accurate determination of aging rates. Our results demonstrate that the storage voltage level strongly influences the degradation rate, with temperature playing a minor role. The identified aging effects include loss of active material on the cathode side and loss of lithium inventory. Initial degradation follows a $\sqrt{t}$-trajectory but is caused by overhang effects. The long-term aging is rather linear.

1. Introduction

Lithium-ion batteries play a significant role in decarbonizing transport, mobility, industry, and household energy consumption. Only a few applications demand continuous cycling. Many applications have long periods of waiting with only intermittent use of the cells, e.g., private vehicles or uninterrupted power supply. For these applications, not cycle performance but calendaric lifetime is essential. A long calendaric lifetime of batteries is also key for resource-efficient product use.

The breakthrough of the lithium-ion battery in so many applications is also due to the introduction of new materials, e.g., nickel-rich cathodes and mixed silicon-graphite anodes for high-energy applications. New materials in lithium-ion cells boost the energy density, increase the capacity, or provide better performance. While cyclic tests typically provide results relatively quickly, the influence of new materials on calendaric lifetime is seldom discussed and even less often published.

This paper investigates the long-term influence of NCA and silicon-graphite on the battery's calendar life. Furthermore, we test the applicability of commonly applied trends and modeling attempts. The structure of the paper starts with a small review of published aging tests with similar cell chemistry to identify which aging behavior to expect. We also include a section about the aging effects on material level, to later compare to the findings of this test. Afterward, the experimental setup is described, followed by the presentation and discussion of the results.

1.1. Aging Data

Calendaric aging data for silicon-containing batteries is not widely looked at, as also McBrayer et al.[2] state. If data is gathered, it might just not be published (yet). To the best of our knowledge, no publication systematically compares various aging conditions over such a long period. Table 1 summarizes publications about calendaric aging which can be found in the literature. The amount of publications in the battery community is enormous, so we do not claim that the table is exhaustive. The table only includes chemistries similar to the cell used in our experiment. Therefore, only publications investigating cells with NMC and NCA cathodes are listed vs. C or C/Si blend anodes. In the following, we will discuss the findings of each publication in Table 1 and summarize their attempt at modeling the aging behavior.

Harlow et al.[3] present a thorough study including cycling and calendaric results. This is one of the few studies using a linear model to project lifetime from their data into the future. Their aging rate is $0.02\frac{\mathrm{SoH}}{\mathrm{a}}$ for the calendaric aging at 40 °C,

[a] F. Frie, H. Ditler, S. Klick, G. Stahl, C. Rahe, T. Ghaddar, D. U. Sauer
Chair for Electrochemical Energy Conversion and Storage Systems, Institute for Power Electronics and Electrical Drives (ISEA), RWTH Aachen University, Campus-Boulevard 89, 52074 Aachen, Germany
E-mail: fabian.frie@isea.rwth-aachen.de
batteries@isea.rwth-aachen.de

[b] F. Frie, H. Ditler, S. Klick, G. Stahl, C. Rahe, T. Ghaddar, D. U. Sauer
Center for Ageing, Reliability and Lifetime Prediction for Electrochemical and Power Electronic Systems (CARL), RWTH Aachen University, Campus-Boulevard 89, 52074 Aachen, Germany

[c] D. U. Sauer
Helmholtz Institute Münster (HI MS), IEK 12, Forschungszentrum Jülich, 52425 Jülich, Germany

[d] D. U. Sauer
Institute for Power Generation and Storage Systems (PGS), E.ON Energy Research Center (E.ON ERC), RWTH Aachen University, Mathieustrasse 10, 52074 Aachen, Germany

[e] D. U. Sauer
Jülich Aachen Research Alliance, JARA Energy, Templergraben 55, 52056 Aachen, Germany

Table 1. Overview of different calendaric aging experiments and modeling approaches reported in Literature.

Author	Chemistry	Test Setup	Reported Testing Time and cell number	Modelling approach
Keil2016[4]	NCA/C NCM/C LFP/C	OCV storage at 11 SoC at 25 °C, 40 °C and 50 °C, storage conditions set by actual capacity	9-10 month	Combined $\sqrt{t}$ and linear model[5]
Werner2021[8]	NCA/C	OCV storage at 5–7 SoC level at 40 °C, 50 °C, 60 °C	24 month	Exponential decay and linear model
Krupp2022[9]	NMC/C	OCV storage at 50 %, 70 %, 90 % at 23 °C and 50 °C	14 month	Exponential model with exponent 0.5-0.789
Harlow2019[3]	NMC (single crystal) /C	OCV storage at 5 Soc level (mostly high voltage levels)	15month	linear fit
Schmitt2017[6]	NMC/C (18650)	OCV storage at 4 SoC level and 0 °C, 20 °C, 45 °C	15-16 month	linear fit
Keil2016a[15]	NCA/C (18650)	study from [4] plus another study OCV storage at 6 SoC levels 25 °C and 55 °C	-	-
Kuntz2021[7]	NCA/C + Si (18650)	OCV and Float storage at 100 % SoC at 45 °C	4.5 month 15 Cells	-
Zilberman2019a[11]	NMC/C + Si (18650)	OCV at 13 different SoC	11 month 13 cells	-
Zilberman2019[10]	NMC/C + Si (18650)	OCV at 70 % SoC at 25 °C	10 month 24 cells	-
Zuelke2021[13]	NCA/C + Si (21700)	OCV at 8 different SoC at 25 °C, 40 °C and 50 °C	12 month 24 cells	-

which equals ten years until an 80 %-End-of-Life criterion would be met. They could not determine an aging rate at 20 °C. One has to note that the chemistry under test was a single-crystal NMC material vs. graphite. This type of cathode has the advantage of having fewer to no crystal boundaries, potentially leading to less electrolyte oxidation, as known from other NMC/NCA cathodes. This study reported storage conditions only at high states of charge. The graphite is therefore always fully lithiated, which is known to increase SEI formation[1] and aging rate.

Keil et al.[4] took a different approach and investigated three different chemistries, one of them NCA/C and another NMC/C, at 16 different SoCs. The study used commercially available cells. It shows that the anode potential is the main driver for calendaric aging. The rate is mainly dependent on the lithiation degree of the anode. For the NCA/C cell, aged at 50 °C and 80 % SoC, they measured 11 % capacity loss in 10 months and at 20 % SoC only 7 % capacity loss. This results in a mean capacity loss in the order of 1.02 and 0.65 respectively. According to their findings, the main aging driver was the loss of cyclable lithium inventory (LLI). Their data was used by Single et al.[5] for modeling purposes. Single et al. fitted a linear model combined with a $\sqrt{t}$-model for SEI growth with a factor depending on anode potential to this data.

Schmitt et al.[6] looked at NMC/C 18650 cells and did a calendaric aging study at four different states of charge for 1.5 years. A linear model was fitted to the capacity aging trend, as it had a better fit than a $\sqrt{t}$-model. This study includes reference cells that did not undergo regular reference performance tests (RPT). These cells retain a higher capacity than the

ones actively monitored, e.g. at 100 %SoC and 20 °C the difference in remaining capacity was 0.98 % vs. 0.99 %. A difference is found for the resistance increase as well. This leads them to the conclusion that the RPT interval influences the measured calendaric aging effect.

A more recent publication from Kuntz et al.[7] compares float and open-circuit storage conditions for cells from different manufacturers. One of the cells they tested is the Samsung 35E, which is also investigated here. All tested cells are stored at 100 % SoC in open-circuit condition or floated at 4.2 V respectively at 45 °C. For the reported 4.5 months of testing, the difference in capacity for both test methods is negligible for this type of cell, which is interesting as the other tested cells show significant differences.

Werner et al.[8] have measured calendaric aging of NCA/C pouch cells under open-circuit condition. They have measured and modeled an exponential decay of capacity followed by linear behavior. This publication stands out, as it provides data for the longest testing time of 2 years. In contrast, all other publications contain data for just over a year, cf. Table 1.

Krupp et al.[9] aged 12 NMC/C pouch cells with a capacity of 64Ah at two temperatures and three states of charge. The resulting data is fit using a model similar to that of the aforementioned publications. A factor depending on storage SoC and Temperature multiplied with time to an exponent is used ($C_{loss} = A(SOC, T) \cdot t^{\beta}$). The exponent value is fitted close to 0.5 for the beginning of the test and overall 0.789. Therefore, this publication is similar to Schmitt et al.[6] and Single et al.[5] They all observe a square root-like behavior for a beginning period and a tendency to a more linear behavior after that.

Two further publications from Zilberman et al.[10] use an 18650 cell with a C/Si anode but with a nickel-rich NMC cathode. They find that a loss of active material during calendaric aging is taking place together with slightly less pronounced LLI.[11]

A publication from Kalaga et al.[12] looks at NMC vs. Si/C cells and compares these to NMC vs. C cells for cyclic and calendaric testing. Calendaric tests consist of a 600-hour constant voltage hold period. Their data show that Si-containing cells age faster than those without Si. Although the potential vs Li/Li^+ is higher for silicon, it seems more reactive than graphite.

One of the few papers looking at the calendaric aging of NCA vs. Si/C cells was written by Zülke et al.[13] They investigated a 21700 cell with an anode, including a similar silicon content as the cell presented here, the only difference was the form factor as the cell was of a slightly larger 21700 format. They found increased aging around 80 % SoC and discussed self-discharge through a shuttle process driven by gaseous CO_2, which reduces SEI growth at 100 % SoC.

To summarize the aforementioned calendaric aging papers, nearly all of them report rather short testing times, around one year on average. The number of cells tested was either not stated or just a few cells were tested, often only a single cell per testing point was used. With a total of 69 cells and 60 months of testing time, the data provided here can provide further statistical relevance. With the provided aging data of about 5 years, no forecasting is needed to identify how long cells will last.

The reviewed papers that try to model calendaric aging[5,6,9] agree that using a root-like behavior to predict calendaric aging is not valid. The long test duration in this paper allows us to separate the initial break-in period from the second linear aging phase and allows to approach similar modeling attempts as in Hildenbrand et al.[14]

1.2. Material Aging

During the operation of the battery, the active material can react with the electrolyte, leading to aging effects. On the anode side, the electrolyte is thermodynamically unstable, especially at high degrees of lithiation of the anode. The reaction leads to the formation of the solid electrolyte interface. During this process, the organic components of the solvents and the lithium salts are consumed, forming Li-carbonates or Li-fluorides and alkyl-carbonates[16] and organic polymeric species.[17] This process is considered the major contributor to calendaric aging, consuming cyclable lithium and increasing the resistance for intercalation into the anode. In severe cases, pore-blocking might occur, which hinders electrolyte and, therefore, lithium-ions from reaching parts of the anode, resulting in loss of active material. Nevertheless, the SEI is a vital part of the battery, and a stable and lasting passivation layer is needed for the cell's longevity.

While the SEI on graphite is thought to become quite stable after some time, it is still under debate how stable an SEI can become on a silicon surface, as the silicon particles undergo drastic volume changes during cycling. The SEI formed on silicon differs from the one on graphite as it seems to be more reactive. McBrayer et al.[2] state that the contact between silicon and electrolyte can lead to a so-called HF-cycle if water traces are present. The cation PF_6- together with water forms hydrofluoric acid (HF). Which in turn etches the SiO particle and forms gaseous species. These gases could block pores on the anode or migrate to the cathode. Silicon oxide is a component found on the surface of silicon particles. This oxygen can be released from the surface and with the HF form water again, thereby closing the cycle. Kalaga et al.[12] describe a similar reaction to produce (HF) from residual water traces. In contrast to McBrayer et al.,[2] Kalaga et al.[12] claim that the reaction with the anode material is thought to consume the HF, forming insoluble components and, therefore, SEI cracking through volume changes of Si could be beneficial in not depleting the electrolyte. Lu et al.[18] conclude from their test results that the SEI on SiO is not calendaric stable and that the cyclic crack-and-repair mechanism might not be the primary cause of aging. Similarly, Yin et al.[16] find a non-passivating SEI on Si. The components in the SEI on Si are described as a thin LiF film on the particle followed by a polymeric layer.[17] According to Veith et al.[19] and Hasa et al.,[20] the SEI layer also "breathes" similar to the volume expansion of the particle and is partially solvable again in the electrolyte.[21] As an additive, FEC changes the SEI to include more polymeric parts, generating more elasticity and

reducing the SEI thickness growth. This seems beneficial but might lead to HF accumulation during calendar aging, according to Kalage et al.[12] Jung et al.[22] find that cells with Si are cyclable with good capacity retention until FEC is consumed, and Bareno et al.[23] stress the positive effect of FEC for a stable SEI attacked by HF.

Expected aging effects on the cathode side of the battery are on a macroscopic level through mechanical degradation in the form of cracking. On a microscopic level, changes in the crystal lattice are reported in literature. Depending on the used materials, either only primary particles can be found, or large secondary particles, which are agglomerations of primary particles, are used. Therefore, three types of boundaries exist: between the primary particles, at interstitial crystal defects, and between crystal grains inside the primary particles. During cycling, the cathode material undergoes small volume changes. This leads to stresses at the aforementioned boundaries, and secondary particles start to develop cracks between the primary particles and open up gaps to be initially wetted by the electrolyte. According to Liu et al.,[24] the electrolyte is oxidized at these surfaces due to the local potential. Furthermore, the crystal structure changes at the surface of the particles. Nickel atoms change to offside positions or are even dissolved in the electrolyte. This leads to an increase in the charge transfer resistance.[25] These surface changes are also known as surface reconstruction layers,[26] which "pin"[27] the layers beneath the surface, disallow expansion and, therefore, reduce storage capacity for lithium, leading to a fatigued phase. Additionally, cross-talk effects due to dissolved transition metals would increase SEI growth on the anode side.[28] While the aforementioned mechanical cracking process is typically initiated by cycling, the aging and consumption of the electrolyte are still relevant for long-term calendaric stability. High potentials at the cathode are known to generate gases by oxidation of the electrolyte.[26,28] This gas can either block pores and cracks of the NCA particles and, therefore, cause impedance rise or travel to the anode side, where it is reduced and consumed in additional SEI growth. The gas evolution at high states of charge is also reported by Hyun et al.[26] For cells aged at 100% SoC, they have found increased gas evolution due to oxygen release compared to cells aged at SoC 70%. They show that the structure of the NMC and NMCA materials remains intact but the lattice parameter c shrinks, Hyun et al. attribute this to oxygen vacancies reducing the repulsion of the layers. They also report a shuttle process due to CO_2 transferring Lithium from the anode side to the cathode, thereby reducing the loss of lithium inventory but degrading the cathode material. In summary, we could expect a loss of lithium inventory and a resistance increase due to SEI growth. The silicon material could attribute to the aging due to a higher reactivity and the promotion of HF-cycles. It is possible that the electrolyte is oxidized at the NCA surface, resulting in the production of gaseous species and the aforementioned NCA material degradation, leading to further resistance increase and dry-out effects.

Experimental

This section presents the cell type, the experimental setup, and its test protocols. The cylindrical cells under test are manufactured by Samsung and labeled INR18650-35E. The cell chemistry consists of a nickel-rich cathode based on an NCA material combined with an anode made of a mix of graphite and silicon. ICP-OES measurements revealed a Ni:Co:Al ratio of 8:1:$<$0.1 and a silicon content of ~3wt-%. The NCA material of this cell consists of small primary particles, which are agglomerated to large μm-sized particles.

According to data sheet specifications, the cell has a minimum discharge capacity of 3.35Ah at 0.2 C or 3.25Ah at 1 C. The 1 C rate is defined as 3.4 A. As this C-Rate defines the testing rates, we have also chosen to normalize all capacity data in this publication with 3.4Ah as nominal capacity. The cathode is fully coated from both sides except for a small area around the current collector. An area of 715 cm^2 was measured for one exemplary cell. Together with the full cell capacity, this results in a theoretical areal loading of $\frac{3.4\ Ah}{715\ cm^2} = 4.75\ mAh/cm^2$. The anode loading calculated from a coin cell measurement results in a 5.8 mAh/cm^2 value. The coated area is measured at 760 cm^2. This results in an overhang area of $760\ cm^2 - 715\ cm^2 = 45\ cm^2$, with an approximate capacity of 265 mAh or around 7.8% total capacity.

The measurement setup consists of 4 ovens kept at 35 °C, 40 °C, 45 °C, and 50 °C, respectively. Each oven has two racks in which printed circuit boards (PCB) are placed onto which the cells are mounted. The cells are soldered to the PCBs using pieces of desoldering braid. Each PCB has connections for the current supply and voltage sense line, resulting in a 4-point measurement setup. The cells are kept at 5 different voltage levels using linear power supplies (HAMEG source meters). Figure 1 shows the described storage of the cells. The voltage levels were chosen the same as the mid-SoC levels for a cyclic aging test, which can be found in Willenberg.[29] Table 2 shows the combination of voltage and temperature and the number of cells at every aging point. The Table also gives the initial SoC, but in contrast to the test in Willenberg,[29] the cells were not kept at a constant SoC but at a constant voltage. This implies that over the time of the test, the SoC slips when the balancing of the electrodes changes due to aging.

In regular intervals, the cells are taken out of the ovens and are electrically tested in a temperature chamber from Binder at 23 °C, with a reference performance test (RPT) as shown in Figure 2(b). The interval was set to two months at the beginning. The interval was increased to three months after the 13th RPT after circa 2 years of testing. After 1.5 years following the 19th RPT (6x3 months), the interval was reduced back to two months. This was done to check the influence of intermittent cycling on the aging rate, assuming that it would decrease with less cycling. The RPT consists of two cycles with a C/2 discharge, followed by a CC–CV charging phase,

Table 2. The table gives the number of cells that started at different test conditions. The SoC is given as a reference but is only valid for test start as it will diverge over the time of the test.

Floating Voltage Initial SoC	35 °C	40 °C	45 °C	50 °C
U1 = 4.054 V 80% SoC	3	3	3	3
U2 = 3.870 V 59% SoC	3	2	2	2
U3 = 3.711 V 45% SoC	3	3	3	3
U4 = 3.510 V 28% SoC	3	2	2	2
U5 = 3.474 V 25% SoC	3	3	3	3

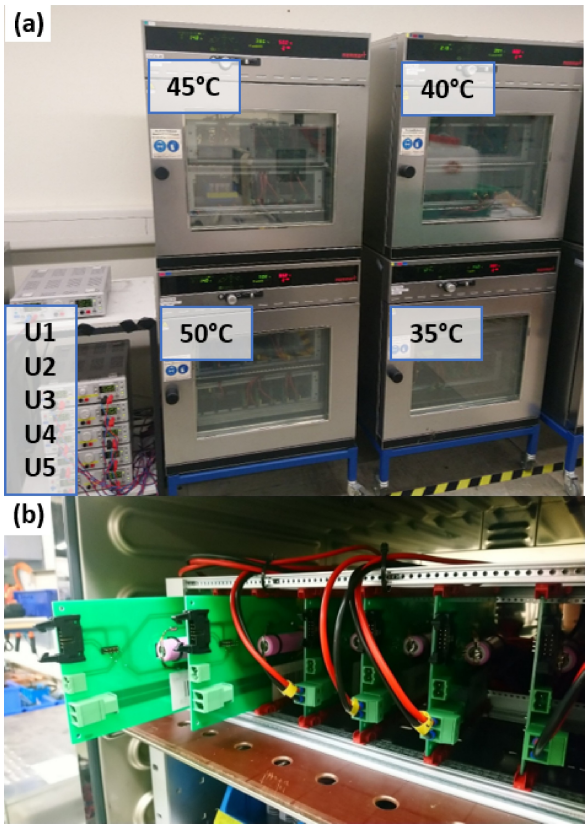

Figure 1. The test setup for storing the cells.
1 (a): 4 ovens at fixed temperatures and the voltage sources on the lower left. Cables from the voltage sources to the cells were run through an inlet on the backside of the ovens.
1 (b): The cells are fixed to a PCB and are stored in racks. The cells were taken out with the PCB boards and connected to the cycler for the RPT.

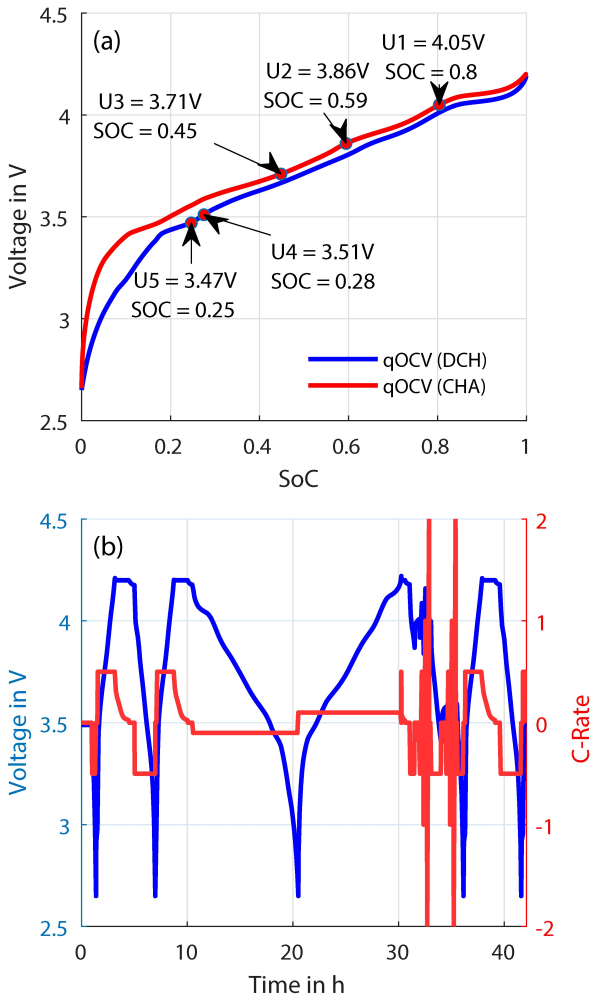

Figure 2. Testing condition and RPT Definition:
2 (a): This figure shows the voltage levels chosen for storage.
2 (b): The RPT consists of a CC–CV full charge after an initial discharge, followed by the capacity measurement. Afterward, the qOCV measurement takes place, followed by two SoC levels (70% and 100%) with a series of pulses. The test setup for storing the cells consists of 4 ovens and the 5 HAMEG source meters on the lower left. The cells were taken out with the PCB boards and connected to the cycler for the RPT.

followed by a slow discharge-charge cycle (C/10), which will be called quasi-open-circuit-voltage (qOCV) in the following. The next cycle includes pulse succession at two SoC levels (70% SoC and 50% SoC) with charge and discharge pulses. The RPT finishes with a discharge and a final charging of C/2 for 20 minutes. The procedure was run on a cycler made by Digatron (Type: MCT 10–06-12ME). After the RPT, the cells are returned to the ovens and held at their specific voltage again. Cells at levels U1-U4 are charged by the HAMEG voltage source, and the cells from level U5 discharge to their respective voltage. When the cells at U4 have lost some capacity, they switch from being charged to discharge, as cells from level U5. The voltage source has a control with a slight offset. The cells stay a little below the set voltage and never switch between charging or discharging during the aging periods in the ovens.

Increased resistance causes an overshoot of the upper voltage limit during the charging pulses at 70% SoC for some aged cells. The cycler is faster in stopping the full test than the program detecting that the pulse step should be aborted. Therefore, the RPT procedure was altered in two ways. The pulses at 70% state of charge were omitted, and the C-rate of the qOCV decreased to C/20. This changed RPT-procedure will be called RPT-EOL (End of life) in the following and is applied to all cells that fail the standard RPT-routine.

In July 2022, the institute moved into a new building, which made it necessary to move the test setup as well. This resulted in not all cells doing a 19th RPT. After restarting the test, RPT numbers were continued at 20. The cells were at ambient temperature and OCV condition during the move for 3.5 weeks.

From the RPT test data, the following information is extracted and discussed in this paper: the discharge capacity, the pulse resistance extracted from a pulse at 50% SoC, and the differential voltage analysis of the charging part of the qOCV.

The complete measured RPT data is available under https://doi.org/10.18154/RWTH-2023-10931. This enables the scientific community to use these data for modeling and plausibility checks. We also encourage fellow researchers to share their data to accelerate scientific progress.

After a significant aging time, cells are opened in argon-filled glove boxes (O_2: <1 ppm, H_2O: <1 ppm) in our analytical lab. Cells were opened at voltage level U1 to identify how much area of the anode is charged to a fully lithiated state, which can be visually detected by the graphite's golden color at that state. Two samples each were taken from the bottom, mid, and top third of the jelly roles height. Coin cells are referenced with B, M, and T for bottom, middle, and

top, respectively, based on the position of the samples used, cf. Figure 9 (c). Top refers to the side of the cathode tab/positive battery terminal. The samples were taken with a 16 mm diameter punch and assembled in a 2032 coin cell format. The coin cells were assembled using a lithium counter electrode and a glass-fiber separator (Whatman GF/C). For further analysis the coin cells were cycled at Neware cyclers (CT-4008T-5V10mA).

The scanning electron microscope (SEM) analysis was performed with a Zeiss Supra 55 using the SE detector and an accelerating voltage of 5 kV. For the energy-dispersive X-ray spectroscopy (EDX) measurements, the Oxford Ultim Extreme was used (accelerating voltage: anode 10 kV, cathode 15 kV). Samples were taken from both electrodes. The SEM/EDX samples were prepared in an argon-filled glove box and then transferred to the electron microscope using a vacuum transfer module (Kammrath & Weiss GmbH). With the transfer shuttle, the specimens were protected, avoiding any contact with moisture and oxygen from ambient air at all times during the transfer process.

2. Results and Discussion

This section presents the results from the electric tests, including the capacity decay, pulse resistance, and differential voltage analysis (DVA). Subsequently, post-mortem results will be discussed.

2.1. Capacity, Resistance and Aging Rate

The capacity of the cells is taken from the first discharge after the CC–CV full charging. The values are normalized with 3.4. Figure 3 shows that a break-in period can be observed for all conditions. The period is at a maximum around 250 days/c. 0.7 years long. This is well visible for the three lower voltages (U3-U5) in Figure3(c)–3(e). During this period, the capacity trend shows a $\sqrt{t}$-behavior. For U2 and U1 in Figure 3(b) and 3(a), the break-in period is disturbed by errors in the test setup. Some cells were not firmly connected, and the voltage source from HAMEG produced a couple of errors at the beginning and did not charge the cells properly. The remaining cell capacity is higher for cells aged at lower temperatures. After the break-in period, capacity decay follows a very linear trend. From the continuous linear trend from year 1 to year 3, we conclude that $\sqrt{t}$-aging models can fit only the first phase dominated by secondary effects but are not suitable for the actual aging behavior. The cells aged at the highest voltage level U1 show the beginning of a knee-point at 70% SoH and thereby the end of the linear phase, further discussions of the knee-point are not the focus of this paper.

For the second period of the aging test (>250 days), aging rates, or the mean capacity loss per day, were calculated using a linear fit. The next ten RPTs after 250 days were used to calculate the slope. The aging rates are shown in Figure 4. The four lower voltage levels form a subgroup with the expected increasing rate for rising temperature and voltage. The cells seem to be quite insensitive to temperature, as the delta of 15 K temperature increase leads to less than twice the rate (0.2 mAh/day increased to 0.38 mAh/day at U2). In strong contrast to this, cells at the highest voltage level U1 show a severely increased aging rate, around 0.5 mAh/day. The increasing temperature leads just to a moderate increase to 0.55 mAh/day. We note, that at least for this cell chemistry the SoC/voltage level is dominating the aging rate. We fitted Arrhenius's law to the data points. The root-mean-square values of this fit are given in the legend of Figure 4. The deviation of the fit from the data is acceptable, nevertheless a linear fit would lead to similar results. Which leads us to the conclusion, that the exponential behavior in this temperature range is not strong. Arrhenius's law was used to extrapolate the aging rates to lower temperatures. At 10 °C, which is just about the average yearly temperature in Germany, the cells would have an aging rate between 0.05 mAh/day to 0.08 mAh/day for the four lower voltage levels. This would result in an aging time of 37 years down to 80% SoH. For the highest voltage level, the extrapolation results in a value of 0.38 mAh/day, so the cell would only last around 5 years. Depending on the use of the cell or at which SoC it is stored, the lifetime expectancy can be very different.

Only a single cell has shown a sudden-death behavior so far, see Figure 3(b). Cell G (cf. Table 4) experienced a sudden drop in capacity after 3 years of testing time. Testing was continued for some time, and the cell stabilized at a low capacity level. Further results of this cell will be discussed in chapter 2.3 and 2.4.

As already seen before, test errors lead to artifacts in the capacity measurement, e.g. during setup of the experiment the cells at U1 and 50 °C were not connected properly to the voltage source. This leads to the inversed behavior of the first two RPT in Figure 3, where the highest temperature curve is above all other levels. Another artifact is visible in Figure 3(c) and 3(d) for the 40 °C test condition. Between 4.5 and 5 one cell aged at U4 loses capacity and one cell from U3 increases in capacity in the RPT next to the last one. One explanation is a wrong assignment of the measurement data to the cells, meaning that data assigned to the cell aged at U3 were actually measured with the cell aged at U4. Another explanation could be a mistake regarding the connection to the voltage source. The cells might have been mistakenly stored at interchanged positions in the ovens. The last explanation would give rise to an interesting hypothesis. One could conclude, that both cells have aged the same and the measured capacity difference is only related to the different storage conditions and induced overhang effects.

Around year four, a slight decrease in the slope is visible in all capacity plots. This decrease is due to the relocation of our testing lab. During that time, the cells were at ambient temperature and open-circuit condition for 3.5 weeks. While lower voltage levels and open-circuit conditions at ambient temperatures decrease the aging rate, the decrease in RPT-frequency did not show a decreasing rate. The same linear slope is continued during the period of less RPT. We cannot rule out that the RPT is without influence, but it gives some confidence that the main driver is calendaric aging.

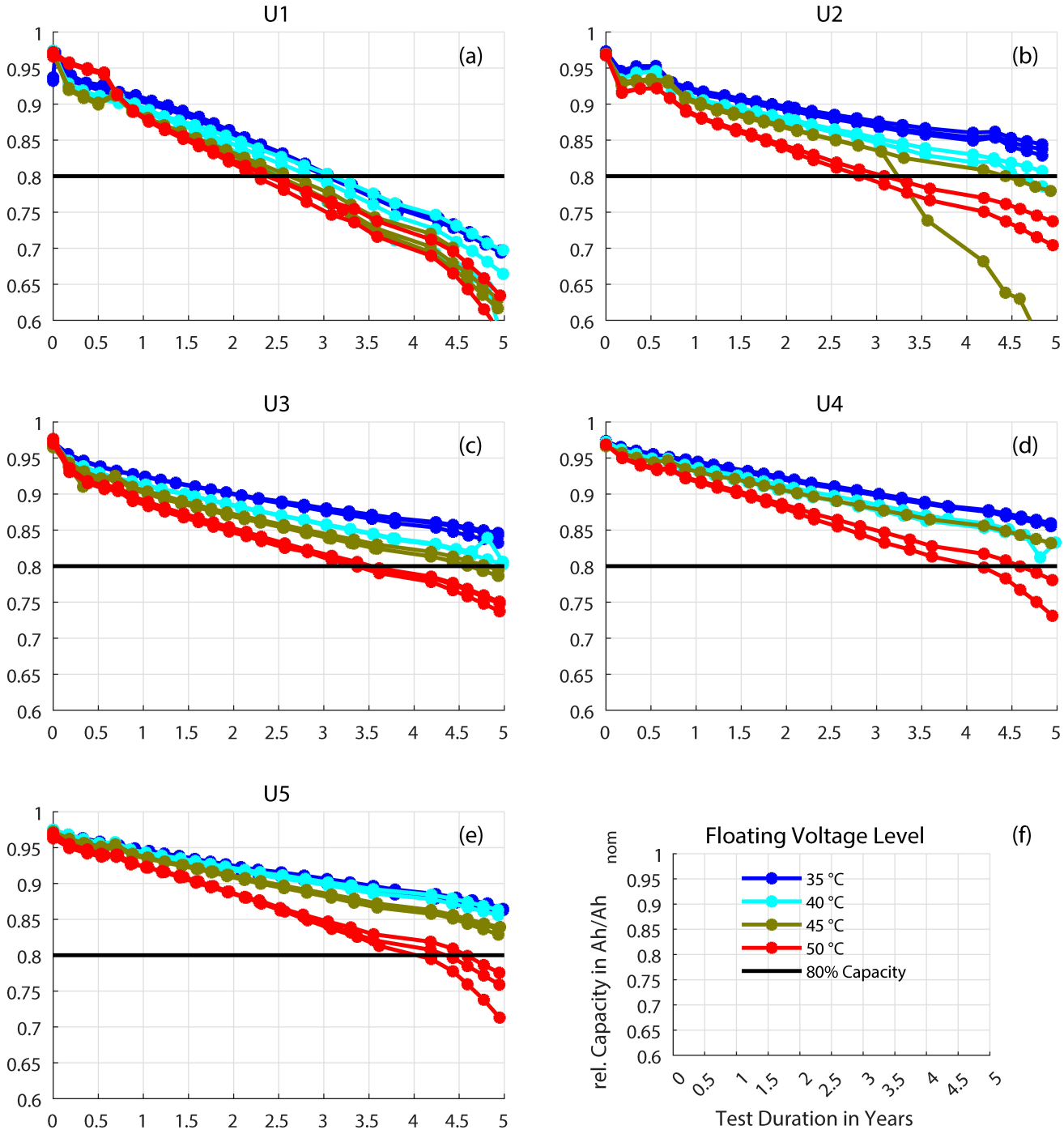

Figure 3. Capacity Trend:
3(a)–3(e): These plots show how the capacity evolves over the testing period, separated by their respective floating voltage levels U1 to U5. All plots show a very linear decline after a certain break-in period. In 3(a), the decline is very similar for all temperatures, while in 3(b) to 3(e), the temperature conditions separate.
3(f): Definition of legend and labels for all plots in this figure

2.1.1. Capacity Loss Versus Resistance Increase

A similar two-phase behavior as for the capacity can be observed from the resistance rise measured by pulses. The evaluated pulses here are 2 C pulses at 50 % SoC, the resistance is calculated from the voltage value after 2 s during the pulse. Figure 5 shows the resistance increase measured from current pulses plotted versus the capacity loss. Assuming that, capacity loss and resistance increase are interlinked, for example, in case of electrolyte dry-out as described by Klick et al.[30] a continuous trend should be visible. Sudden changes in this trend would translate to different aging processes.

In Figure 5, all cells start with an initial resistance of around 34 mΩ. Depending on their voltage level, a certain capacity

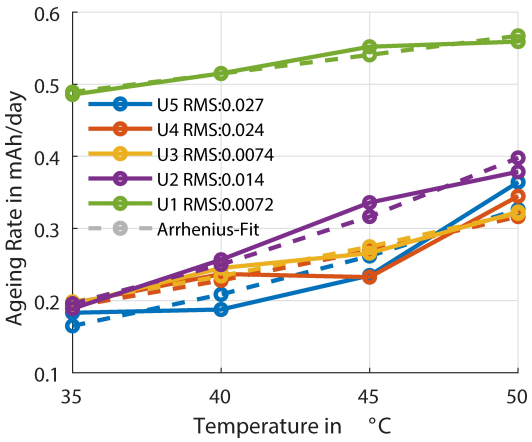

Figure 4. Aging Rates: From a linear fit to the capacity trend, aging rates were calculated. The rates can be fit by an Arrhenius-law with small Root-Mean-Square Values to the temperature increase.

fade preemts a significant increase in resistance. The first nearly constant phase is identical to the initial phase of the capacity plots discussed previously. If SEI growth would be the main contributor to capacity loss in this first phase, we would expect a resistance increase right from the beginning. The start of the second phase depends on the voltage level of the cells. The higher the voltage level, the more lithium can diffuse into the passive overhang areas, which explains the longer first phases. Especially considering the lower voltage gradient between overhang areas and the rest of the cell at high SoCs due to the voltage plateau of the anode. Cells were delivered with 3.48 V, very close to U4 and U5. These two voltage levels also do not show a significant first phase. Cells at U1 lose up to 0.2 Ah during the first phase (4 RPTs, 250 days). From the aging rate, a calculated amount of 0.132 Ah is lost during 250 days. The loss into the capacity of the overhang should be around the change in SoC multiplied by the capacity of the overhang, which results in $55\%\Delta SoC \cdot 265\,\text{mAh} = 0.145$ Ah. The sum of both is higher than the measured capacity loss. Nevertheless, part of the overhang might be reversibly usable during capacity measurement. As the first phase is dominated by capacity loss and not resistance increase we suggest, that this behavior is more likely due to the overhang effect described by Lewerenz et al.[31] and not a decaying SEI growth. Once the lithiation of the anode overhang has adjusted to the rest of the anode the actual aging process is showing. After the first phase, the pulse resistance increases linearly to the capacity loss. A straightforward explanation would be a symmetric dry-out of the full cell. More and more active particles are only reachable through electrolyte pathways with a high impedance, reducing the capacity of the anode and cathode, additionally, less surface area is available for the current increasing the resistance proportionally.[30]

2.2. Cell to Cell Variation

In the previous sections the trends how capacity and resistance evolve over time, for the whole aging matrix are discussed. In this subsection, we present how cells, that were aged at similar conditions vary in these values between each other. In Figure 6(a) the maximum capacity difference for cells that aged at similar temperature and voltage level are plotted. The capacity difference is normalized by the reference capacity of 3.4 Ah. The majority of cells are measured with a difference below 1%. This low fluctuation between the cells, is a sign for a decent production quality of the cells. Only a few cells show significant deviation after some time. This includes the sudden-death cell, which is visible in Figure 6 (a) as an outlier at the 20th RPT. Cells aged at U1 and 40 °C, start to deviate from each other after the 10th RPT, while for other cells at U1 and to lesser extend also at U2 the deviation increases starting with the 15th RPT. The increase in capacity difference after the 15th RPT, is presumably induced by the increased aging at high voltage levels U1 and U2 and the elevated temperatures 45 °C and 50 °C. The reason for the higher deviation in the case of 40 °C is caused by a single cell. Thus we assume this to be a behavior that can be related to this specific cell rather than the testing conditions (U1, and 40 °C).

Similarly to the capacity, the maximum difference in resistance was calculated and divided with the initial resistance R_0, which is 34 mΩ. At most conditions, the cells show a difference below 10%. The measured spread stays fairly constant over all RPT. This is different to the capacity measurement, which show increasing differences between the cells for the later RPT. Only for cells at U1 and 40 °C, which also are noticeable in the capacity plot, the resistance spread continuously increases. This is due to a single cell, being an outlier to the rest of the cells. The very continuous and smooth behavior of the resistance spread for all other conditions, gives confidence, that the resistance measurement by pulses is very reproducible and feasible.

2.3. Aging According to Differential Voltage Analysis

In this section differential voltage analyses (DVA) of the slow charge part of the RPT will be used to analyze the aging mechanism, and to determine if only loss of lithium inventory (LLI) is present or also loss of active material (LAM) can be found. The qOCV data are fitted by a smoothing spline for noise reduction using Matlab. The numerical derivative of the spline is taken to create the DVA. Figure 7(a) shows the DVA for the full cell and the cathode and anode half-cell. The plot defines labels for the minima and maxima of the DVA curve, which are used in the following analysis. During the charging of the full cell, the anode features A1 to A3 are clearly visible, while the characteristic graphite plateau change A4 is hidden under the cathode feature C2-C3. During aging, the A4 peak becomes less pronounced and smears out, making it even more difficult to track. Towards the end of the charging process the cathode features C3 to C5 are again easy to identify and are persistent throughout the whole aging time. The anode feature A* is characteristic of silicon and will be discussed in 2.3.

Depending on the aging effect, the position of the peak should change differently. Assuming active material loss (LAM)

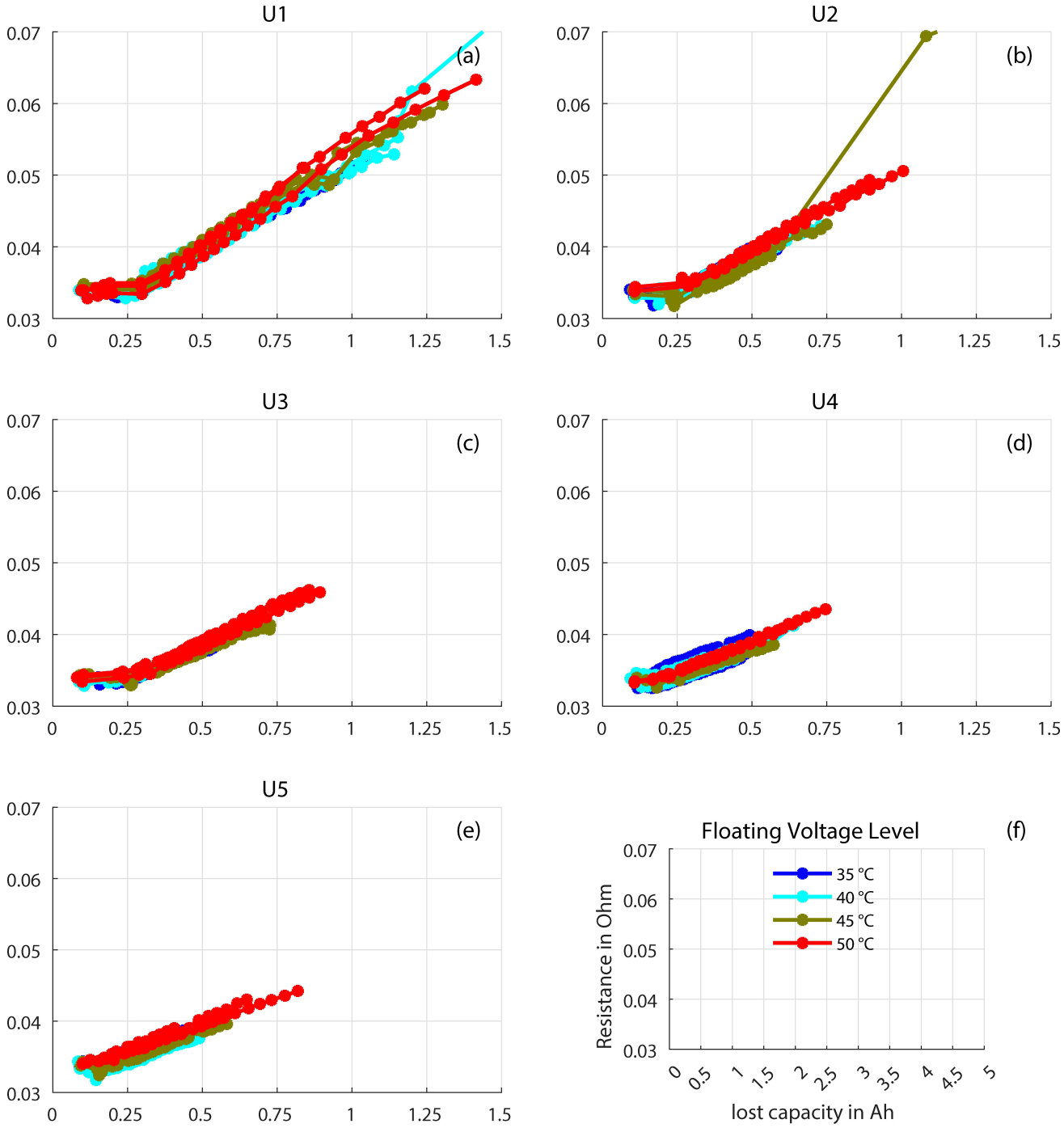

Figure 5. Resistance Increase:
5(a)–5(e): Graphics show the 2 s-Pulse-Resistance for 2 C charging pulses at 50% SoC. The increasing resistance is plotted versus lost capacity for the different voltage levels. U1 to U3 (Figure 5(a) to 5(b)), show that the resistance increases with two different slopes. At the beginning the resistance increase is nearly flat. The higher the voltage level, the longer the first initial loss phase without a significant resistance increase.
5(f): Definition of legend and labels for all plots in this figure.

on one electrode should lead to peaks of the defective electrode moving closer together. The shape stays the same but is squeezed into a smaller Ah range. Therefore, the distance between the peaks C3 and C5 ($\overline{C3C5}$) relates to cathode material loss, and $\overline{A0A2}$ characterizes anode material loss. The loss could be either due to not being connected to the electrical network or insufficient contact with the electrolyte. Also, severe changes in the active material would lead to active material loss. A dry-out of the electrolyte should symmetrically influence the anode and cathode. The curve should be shrinking synchronously and keeping the balance between the electrodes. A distance change between the peaks of the two electrodes is attributed to the LLI. The electrodes shift versus each other and change their balance between them. The

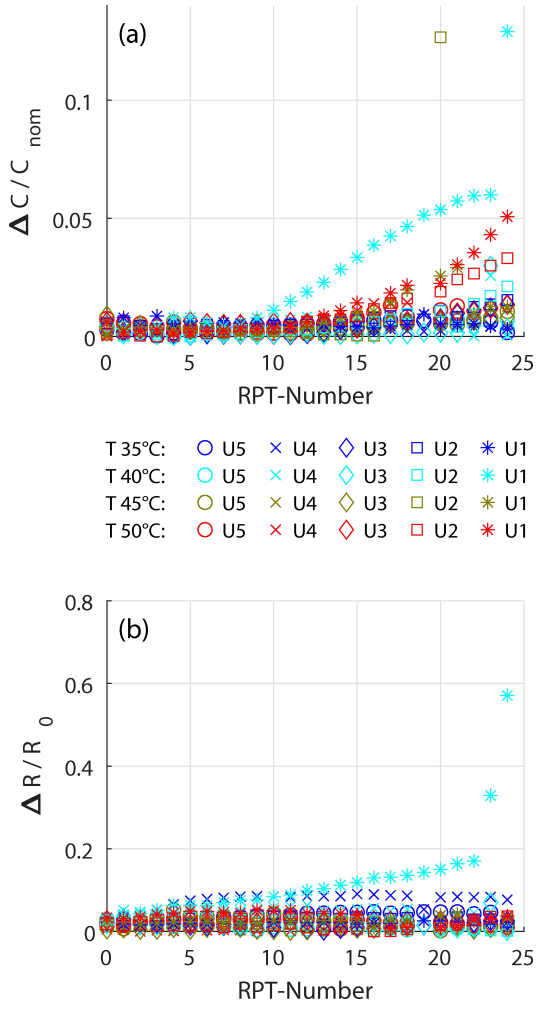

Figure 6. Variation of the measured capacity and resistance values between cells at identical aging conditions, plotted versus the RPT-number:
6(a): The plot depicts the maximum capacity difference measured between two or three cells at the same aging condition, divided by the reference capacity of 3.4Ah. The majority of cells age very similar to each other, with a maximum deviation below 1%.
6(b): The plot shows the maximum difference for the resistance measurement between two or three cells at the same aging condition. The value is normalized by 34 mΩ, as a reference value.

distance $\overline{A2C2}$ is used as an indicator for LLI. The distance $\overline{A0C6}$ is simply the full cell capacity measured with the slow discharge. The values of these measures are given in Table 3.

Three aging conditions have been chosen for further discussion. The first point is the harshest aging condition with U1 at 50 °C. The second condition is the opposite at U5 and 35 °C. The last condition is the aging point at U2 and 45 °C, which is at the highest voltage level of the lower group and also includes the cell with the sudden capacity drop. The DVA plots in Figure 7(b) to 7(d) are plotted on purpose with an offset on the y-axis representing the aging time. The offset is calculated by the testing time multiplied by a factor. Coloring from blue to red also relates to aging time. The absolute values on the y-axis are not relevant for our analysis as we rely on the peak-positions on the x-axis to interpret the data. A jump in capacity can be seen when the RPT routine is changed from a

Table 3. Quantitative changes for characteristic measures of the DVA.

Fig	$\overline{A0C6}$/Capacity	$\overline{C3C5}$
7(b)	3.31/2.49/-24%	0.70/0.56/-4%
7(c)	3.32/2.56/-22%	0.71/0.55/-5%
7(d)	3.31/2.98/-10%	0.69/0.65/-1%
	$\overline{A0A2}$	$\overline{A2C2}$
7(b)	0.79/0.84/2%	0.92/0.32/-18%
7(c)	0.82/0.82/-1%	0.87/0.36/-15%
7(d)	0.80/0.83/1%	0.89/0.57/-10%
	Peak distance in Ah and delta in %-nom. Cap. fresh/old/△	

C/10 to a C/20 rate as described in the experimental part, the position of the peaks does not seem to be too much influenced by this.

Figure 7(b) shows the DVA for the harshest condition (U1, 50 °C). The distance from C3 to C5 is shrinking significantly by 0.12Ah which is 4% of the nominal capacity. The distance $\overline{A0A2}$ is close to constant. According to the measurement, it even seems to increase by 1%. We explain this effect by the broadening of the peaks due to SEI growth, which makes an exact identification of the peaks difficult. From this, we conclude that we have a significant loss of active cathode material and a very stable anode material. The distance $\overline{A2C2}$ decreases continuously for this cell. At the initial state A2 and C4 overlap, later C4 can be found left of A2. While C4 moves to the left, the A2 peak diminishes more and more. Presumably, it reappears between C3 and C4 at the latest RPT in the orange and red lines. The transfer between C3 to C4 is smooth at the beginning of the tests and starts to show a small slope change for the later RPT. The distance $\overline{A2C2}$ changes by 18% of the nominal capacity, which is equal to a large LLI.

The cells aged at (U5, 35 °C) in Figure 7(d) differ to the cells at U1 and 50 °C. The distance between the cathode peaks $\overline{C3C5}$ stays fairly constant (−1%). The anode features ($\overline{A2C2}$) do not change either (1%). So no significant LAM can be detected. The C2/A4 peak broadens, thereby shortening the distance $\overline{A2C2}$, hinting at LLI. The capacity loss of 10% is nearly identical to the distance change of $\overline{A2C2}$, resulting in LLI being the main driver of capacity loss in case of lower voltage levels. Similar results with only LLI as aging effect were also found by Keil et al.[15] for a NCA/C 18650-cell and also by Wojtala et al.[32,33] for exactly the cell used in this study.

In Figure 7(c) the cell with the sudden capacity loss is included (dashed lines), together with the other cell aged at the same conditions (solid lines). The cells age similarly up to the 17th RPT, which is plotted in orange. The 17th RPT of cell G was not successfully completed. Analyses of the 17th RPT show a sudden voltage drop during charging and a massive temperature increase, which could be a sign of an internal short after a plating event. Due to the interrupted RPT, qOCV-data for Cell G was not recorded and the respective DVA is therefore not included in the Figure, only the solid orange line of the other

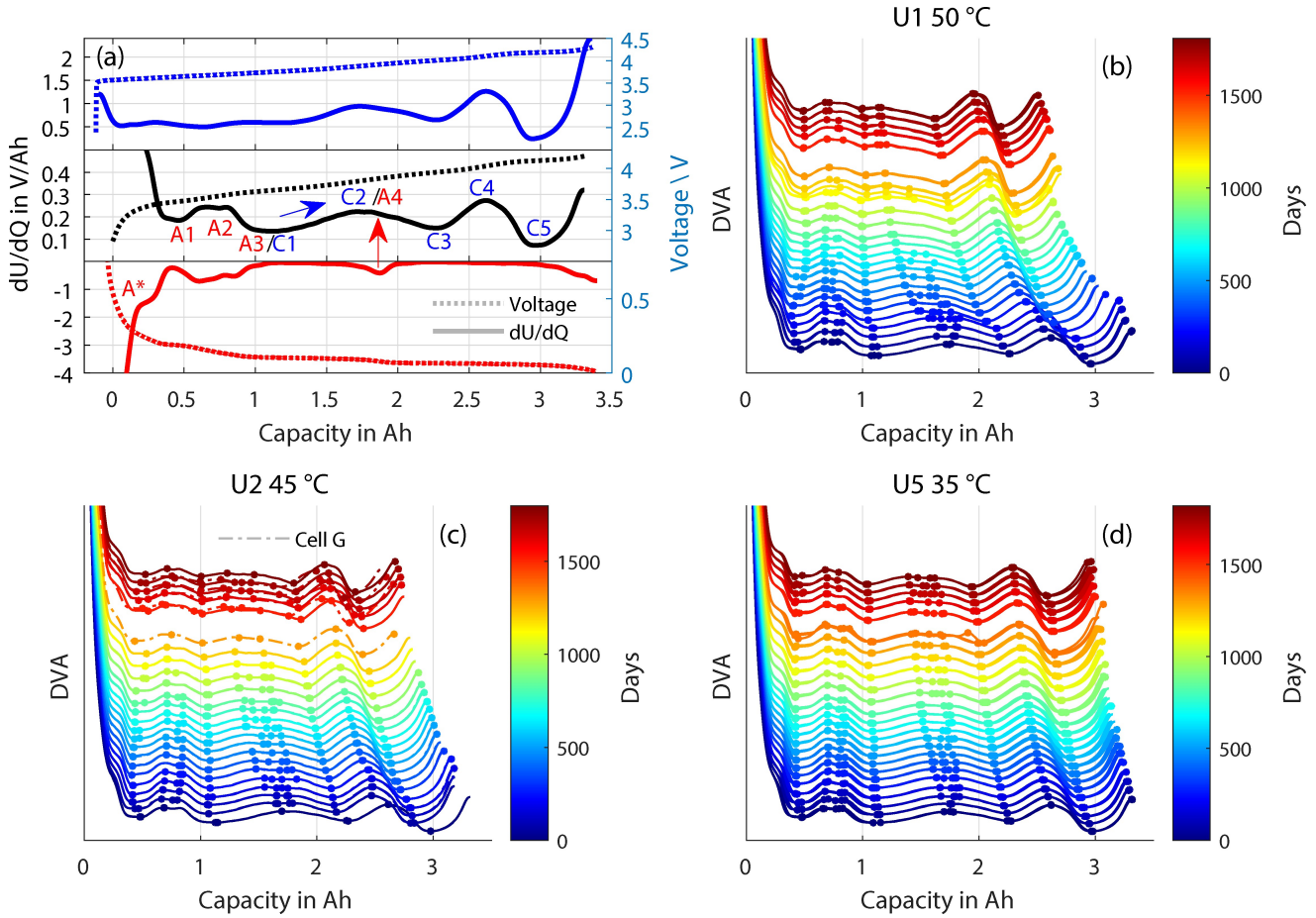

Figure 7. Combination of DVA plots for three selected aging conditions:
7(a): Shows the DVA of the cathode half cell (top), anode half cell (bottom), and the full cell (mid), matching the labeled features of the anode and cathode to the full cell.
7(b): Shows the data for two cells stored at the harshest conditions. The cathode features C3 to C4 are clearly slipping to the left
7(c): Shows the DVA for the condition where one cell experienced a drastic failure. The cells obviously deviate after the failure
7(d): Shows the weakest aging condition. The form and position of all features stay nearly constant the whole time.

cell is visible. Nevertheless, Cell G was kept in the test. During the 18th RPT the electrical tester had a fault and only cell G completed the RPT but not the other cell, therefore only an orange dashed line is visible, and no solid line. After moving of the institute the RPT continued and a massive difference between both cells is visible. In contrast to the other cell (solid lines), cell G shows a 15% capacity decrease between fresh and old state for the distance $\overline{A2C2}$, which results from LLI. A plating event would lead to such a balancing shift. The cathode active material shrinks by 5%. This is true for cell G and the other cell. An anode active material loss is again not visible.

In summary, the cells do not lose active material on the anode side, which is in agreement with other literature findings for calendaric aging. Cathode material loss is detected at U1 and U2 at temperatures above 45 °C, which was not reported by other studies. LLI is the main aging factor according to the DVA results and at low voltage levels the only aging factor.

2.3.1. Silicon Aging

In this subsection, we would like to focus on the Si part of the anode material. One of the characteristics of Si is the hystereses and the feature A0, which is best visible in comparison between charge and discharge. Therefore, Figure 8 uses the slow charge

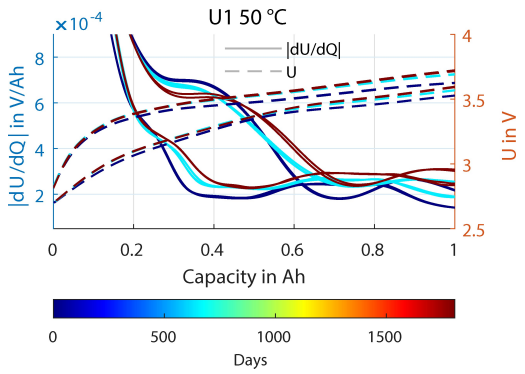

Figure 8. Si behavior over aging time as DVA and voltage plot

and discharge and focuses on the part where the silicon is active. The plot shows the slow charge/discharge curves at begin of life, mid of life and from the latest RPT. In the voltage plot, the hysteresis is consistent even after long-term aging. Also in the DVA, the characteristic peak stays visible and only becomes a little sluggish as does the whole DVA but there is no tendency to lose the Si features, as it happened in cyclic tests of the same cell which are reported by Willenberg.[29] From the electrical perspective, the silicon stays active and keeps its capacity over time.

2.4. Post-Mortem Results

In the following, the results from the cells which were opened during post-mortem analyses are presented. During the opening of cells at a charged state, one could observe that the anode is only partially and very inhomogeneously used, as only parts of the anode show a golden color and are fully lithiated, while others parts appear black and seem not or only partially lithiated. The cells show a tendency to form a stripe at mid-height of the cell. The parts at the top and bottom of the anode seem to be less used, cf. Figure 9(a) and 9(b). This could be due to a couple of reasons: The electrical contact to those particles is lost, the ionic pathways are ineffective due to dry-out effects or a cover-layer has formed causing high impedance.

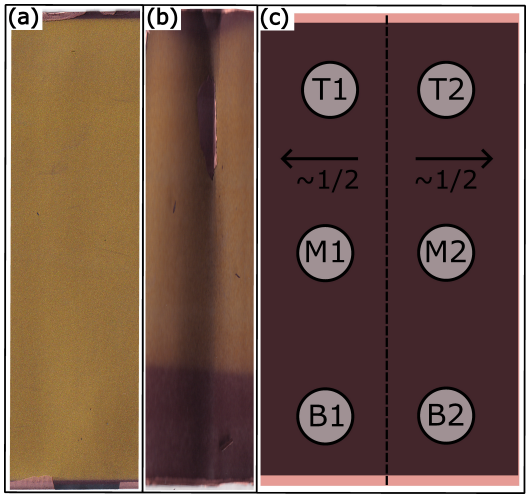

Figure 9. Comparison between fresh and aged anode samples.
9(a): fully charged fresh anode
9(b): fully charged aged anode, with clear inhomogeneous use
9(c): Sample Position and labeling, for the harvested coin cell material.

From a mechanical perspective, the active cathode material stays intact during the post-mortem, with the exception of cell G. This cell experienced the sudden-death, was opened, and the cathode material completely disintegrated and fell off the aluminum current collector.

The anode electrode can never be unrolled without loss of active-material. The active material does not stick to the current collector but crumbles. This effect is more pronounced in the inner third of the jelly-roll, where the radius is smaller, the top and bottom overhang, and on the single-sided outer section of the jelly-roll.

2.4.1. Coin Cell Measurements

To further identify the inhomogeneity of the electrodes, samples are harvested and reassembled into coin cells. The aim is to determine the remaining active lithium at different positions of the electrode and to check the condition of the active material. From the top, mid, and bottom height of the electrode, samples are taken at approximately mid of the electrode length. Samples from the cathode were taken at approximately the same spot, opposing the anode samples. The anode and cathode samples were assembled in coin cells vs lithium. Anodes were cycled between 10 mV and 1.5 V and cathodes between 3.2 and 4.2 Volts with a current of 0.25, which is close to a C/40 rate. First the coin-cells were charged, delithiating the active material harvested from the cell. The addition of this first charge capacity of the anode and cathode sample is a measure of the active lithium at that sample position in the cell, given in Figure 10(a). The labeling of the coin cell data follows the naming convention in Table 4, which also lists the aging conditions of each disassembled cell. The green line in the Figure is the resulting (delithiated) capacity averaged over 6 cycles of an anode harvested from a fresh cell. The added anode and cathode capacity from cell F nearly reaches this reference, although it has aged by 13%. Cell E, which is down to 70% SoH, shows nearly the same amount of lithium (6-7 mAh) in the Anode, but not in the cathode. This aligns with the LLI at high states of charge found in the DVA. For Cell G, which showed the sudden drop in capacity, only two cathodes could be sampled at non-defined positions and two

Table 4. Cells from this Table were disassembled and analyzed.

Cell	Number	Test Condition	SoH [%-Cap]	Aging Time [d]	Ah-Throughput	Last-Checkup
A	273	–	100%	0	0	0
B	247	U1, 50 °C	75.3%	1171	242	17
C	205	U1, 35 °C	77.1%	1359	307	19
D	225	U3, 40 °C	84.41%	1373	272	19
E	233	U1, 45 °C	70.0%	1616	299	21
F	216	U5, 35 °C	87.2%	1757	318	23
G	235	U2, 45 °C	58.6%	1737	287	23

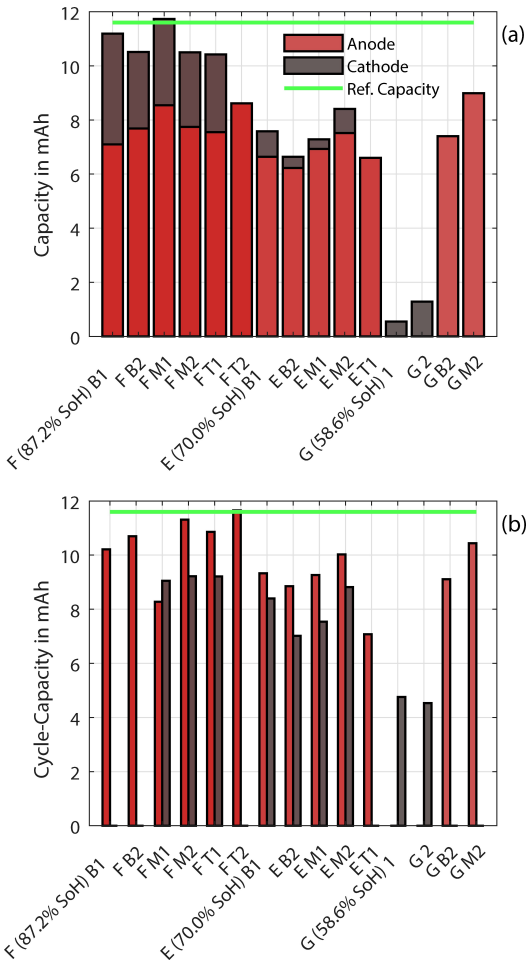

Figure 10. Results of coin cell cycling experiments:
10(a): Combined extract-able lithium from anode and cathode half cell by charging
10(b): Capacity retention at 4th Cycle for anode and cathode half cells.

anode samples (B2 and M2) did cycle. The anode ones show a similar active lithium inventory as cells F and E. The disintegrating cathode has a similar initial lithium capacity as cell E but does not match up to cell F. In contrast, the anode samples of cell G contain nearly as much cyclable lithium as cell F. Position-wise, it is noticeable that cathode samples taken from the top tend to fail (F T2, E T1, and T2), and anode samples taken from the mid position contain slightly more lithium than from top or bottom position. This aligns with the visible in-homogeneity of the anodes' coloring.

Further cycling of the coin cell allows extraction of the full available material capacity of the sample. The fourth cycle was used for evaluation. The results are given in Figure 10b. The capacity is measured above 3.5 V for the cathode and below 0.5 V for the anode, similar to the balancing in the full cell. For Cell F, which has the highest SoH and the active lithium nearly reaches the reference capacity during the first charge, the cycle-capacity of the samples is similarly high. Nevertheless, cathodes from position T2 did not cycle, and B1 and B2 did not reach 4 cycles. For cell E, which has a clear drop in active lithium visible in comparison with cell F the cycle capacity is also reduced for anodes and cathodes and does regain some capacity (1–2 mAh) compared to the initial cycle. Again cathodes T1 and T2 did not cycle, also anode T2 was a failure. For cell G the anodes included nearly as much lithium as the other cells, and with the added electrolyte and lithium chip even gained nearly full capacity during cycling, while the cathodes show a very decreased cycle capacity. This also hints at a cathode degradation mechanism, as also predicted by the previous DVA analyses. The capacity recovery of the anodes is in line with the DVA analyses showing no or only a small LAM for the anode material.

Two results can be taken from this, aging over the electrode area is quite in-homogeneous. In tendency, anode material might be the cause of the lithium loss due to SEI growth, but most of its capacity can be retained if wetted with fresh electrolyte and provided with a lithium source. Therefore, dry-out effects are a likely cause for the inhomogeneous use of the anode. The cathode material seems to have some further degradation effects, as it is more difficult to gain some capacity out of it.

2.4.2. Scanning Electron Microscopy

To gain further insights into the aging of the active material SEM-/EDX examinations were conducted. In Figure 11 and the related Table 5, the results are shown. For the cathode, over an SoH range from 100 % to 58.6 %, no clear visible morphology change such as cracking of the secondary agglomerates can be seen in the top-down SEM examination. This behavior has already been reported in the literature for similar aging conditions.[7] EDX elemental analysis of the cathode shows a relative increase in fluorine and phosphorus in the aged cells compared to the unaged reference (Cell A). The relative increase could be an indicator that the cathode-electrolyte interphase (CEI) has grown since the two elements are often mentioned as part of the interphase.[34] We note that the samples were not washed prior to SEM/EDX and thus contain residual LiPF6, affecting the results. Therefore, further studies with additional methods e. g. X-ray photoelectron spectroscopy (XPS) need to be performed to confirm CEI growth.

The anode, on the other hand, showed more significant aging visible by morphological surface changes. To clearly distinguish between silicon and graphite particles, EDX mappings (Figure 11 bottom) are used. In the unaged state (Cell A), the silicon particles still have a smooth surface and partly a spherical structure. In the aged state, the silicon particles are cracked and an impure surface appears. To illustrate this characteristic, a close-up window with an unaged/aged silicon particle is shown in Figure 11. We assume mechanical aging of the silicon particles, caused by a strong volume change of the silicon (up to 280 % for pure silicon[35]). The EDX comparison of the silicon particles reveals that the unaged particles have more carbon and less oxygen, fluorine, and phosphorus compared to the aged particles. At the moment, it is not yet clear whether the initial amount of carbon is a form of intentional coating or initially formed SEI. However, after the silicon particles are

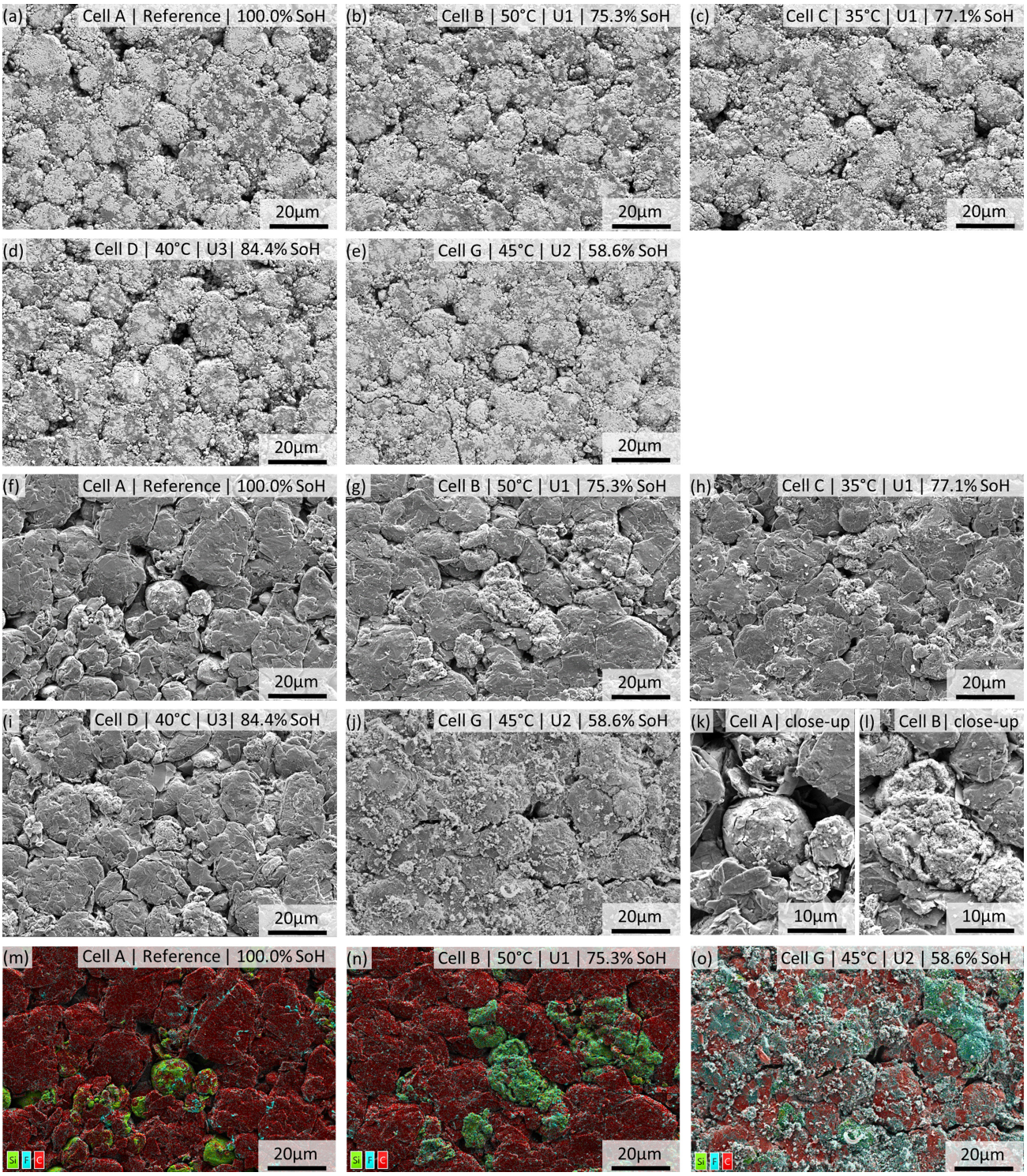

Figure 11. Scanning electron images (SEM) of the cathode and anode surface with a magnification of 1000x:
11(a)–11(e): Cathode surface images of differently aged cells (various voltage levels and temperatures) opened at different SoH.
11(f)–11(j): Corresponding images of the anode surface.
11(k)–11(l): A close-up comparison of the silicon particles of cell A (pristine) and B (aged)
11(m)–11(o): EDX mappings of anode surface from cell A, B and G. These mappings provide a clear distinction between silicon and graphite particles. In addition, a significant increase in fluorine on the surface of a strongly aged cell G can be observed.

cycled and fractured, the O, F, and P content of these particles increases, indicating strong SEI growth. The same SEI formation is also observed throughout the entire anode. With decreasing SoH, the amount of relative oxygen, fluorine, and phosphorus increases on the anode surface. This SEI growth at higher temperatures is widely reported in the literature.[7,36,37] Besides

Table 5. EDX element distribution data of cell A–D and H split by anode and cathode. For the anodes, additional separate measurements were performed for the silicon and graphite particles. All values are given in relative weight percent wt%.

			Cathode		
Element	Cell A	Cell B	Cell C	Cell D	Cell G
Ni	41.6	40.3	40.2	39.5	37.3
O	23.6	21.9	22.5	22.9	24.2
C	21.1	21.2	21.5	22.0	21.6
Co	7.6	7.4	7.3	7.1	6.7
F	4.5	7.1	6.9	7.0	8.0
Ba	0.4	0.6	0.3	0.4	1.0
Na	0.4	0.2	0.2	0.2	0.2
P	0.4	0.8	0.7	0.6	0.8
Al	0.3	0.4	0.3	0.3	0.2
S	0.1	0.1	0.1	0.0	0.1
			Anode		
Element	Cell A	Cell B	Cell C	Cell D	Cell G
C	88.6	75.7	77.5	81.7	54.5
O	5.0	13.1	12.1	10.6	25.2
F	3.4	6.8	6.8	4.3	15.8
P	0.5	2.7	1.6	1.1	3.1
Si	2.3	1.6	1.9	2.2	1.4
Na	0.1	0.1	0.1	0.1	0.1

					Anode			
	Cell A		Cell B		Cell C		Cell D	
Element	Graphite	SiOx	Graphite	SiOx	Graphite	SiOx	Graphite	SiOx
C	97.3	62.6	90.6	46.3	89.4	41.9	90.9	47.8
O	1.6	10.1	5.9	24.1	6.6	21.7	5.4	23.5
F	1.0	6.4	2.7	10.1	3.3	13.5	2.8	8.9
P	0.1	1.0	0.7	3.5	0.8	3.6	0.9	2.8
Si	0.0	19.1	0.0	15.6	0.0	19.1	0.0	16.5
Na	0.0	0.9	0.0	0.4	0.0	0.2	0.0	0.5

the increase of SEI elements on the graphite, the particles do not show strong morphological changes in contrast to the silicon. For cells A–D, the graphite surface looks clean, and only for the most aged cell (Cell G), the entire anode is covered with impurities (mainly based on O, F, and P).

The SEM-/EDX results do not give further insight into the cathode degradation mechanism. Cracking of the particles and adherence losses between secondary particles are not observed. Therefore, we can assume that either changes in the crystal structure not visible to the SEM might be the cause for losing vacancies for the lithium to intercalate, resulting in active material loss[24,25,28] or blocked ionic pathways due to gases generated by electrolyte oxidation lead to the failure. Nevertheless, in the coin cells, the rewetting does not regain full capacity, so some crystal changes are likely. For the anode material, the silicon shows more pronounced residues and cover layers from electrolyte degradation products than the graphite. Nevertheless, as shown before electrically the silicon stays active, so silicon might be beneficial in the sense that the graphite stays cleaner, cyclable, and reusable in the cells.

3. Conclusions and Outlook

With this paper, we provide the aging data over 5 years of calendaric aging at 5 different voltage levels and 4 temperatures for a lithium-ion cell with a Ni-rich chemistry and a Si/C anode. The analysis shows that calendaric aging tests need at least a year to overcome the effects of the passive overhang areas of the anode and afterward show a linear aging behavior. Thus, modelling of long-term aging requires long-term measurements capturing not only the initial capacity loss due to the anode overhang but also the linear decline that follows. This long-term test data also provide a good opportunity for existing calendaric models to be tested and verified.

The temperature dependence of the measured aging rates can be modeled by Arrhenius-Law, but the temperature influence is modest. The voltage dependence is two-fold. For the voltage levels U2-U5 (3.870 V–3.474 V) a similar aging rate between 0.2 $mAhd^{-1}$ at 35 °C and 0.4 $mAhd^{-1}$ at 50 °C are observed. At U1 (4.054 V, initially 80 % SoC) the aging rate is substantially higher with 0.5 $mAhd^{-1}$ at 35 °C and 0.6 $mAhd^{-1}$ at 50 °C.

The main aging driver in this study is the loss of lithium inventory, as would be expected during calendaric aging. Furthermore, loss of cathode material was found by DVA analysis at the highest voltage level U1 and less pronounced at U2. This is in line with the accelerated aging rate, which is measured at U1. This is similar to the results found in Ref. [13] and it is likely that at this voltage level another aging process takes place. It is reasonable to assume that the rapid decay is driven by a cathodic effect, as the loss of active cathode material which is present in the DVA analysis suggests. Oxidation effects at the cathode lead to crystalline changes in the material and, therefore, fatigue of some active cathode material, as explained by Hyun et al.[26] Additionally, the consumption of electrolyte and the generation of gases could lead to the dry-out effects on the anode and cathode. This would result in the inhomogeneous use of the anode, as was shown by the post-mortem results. The active material is not lost but cannot be used to its full extent. The silicon particles of the anode, crumble and attract the formation of SEI and other residues as visible in SEM results, but the Si hysteresis is visible in the DVA until the very last RPT.

First, cells seem to develop a knee-point. We plan to conduct further post-mortem analyses to identify the cause. Further analytics are ongoing to identify the crystalline state of health of the cathode material and electrolyte is extracted for further analysis.

We want to encourage the community to do more investigation of the electrical data or use the provided data to parameterize and challenge their respective lifetime prediction models.

Author Contributions

The individual contribution of all authors is given below, following the Taxonomy of CRediT (https://credit.niso.org/).

FF: Conceptualization: Lead; Data curation: Lead; Funding acquisition: Equal; Investigation: Equal; Methodology: Lead; Project administration: Equal; Visualization: Lead; Writing – original draft: Lead; Writing – review & editing: Lead

HD: Data curation: Supporting; Investigation: Equal; Visualization: Supporting; Writing – original draft: Supporting; Writing – review & editing: Equal

SK: Writing – review & editing: Equal

TG: Writing – original draft: Supporting; Writing – review & editing: Supporting

GS: Funding acquisition: Equal; Project administration: Equal; Writing – review & editing: Equal

CR: Funding acquisition: Equal; Project administration: Equal; Writing – review & editing: Equal

DUS: Funding acquisition: Supporting; Resources: Lead; Supervision: Lead

Acknowledgements

This work has received funding through public funds. The test was continued even after the funded projects ended. Funds were received through the German Federal Ministry of Education and Research through the projects “Meet Hi-EnD II” (03XP0084B) and “Meet Hi-EnD III” (03XP0258C). Additional support was received through the research training group “mobilEM” (GRK 1856/1 1856/2) and the “BaLD” project (03XP0320A). During 5 years of testing, a couple of people had contact with either the setup or the data. The authors thank the following colleagues for fruitful discussions throughout the years, in particular M. Junker and H. Laufen. Also, thanks to the students J. Brucksch, M. Finke, E. Ilbi, and T. Ghaddar who helped to set up and maintain the tests, worked on the analysis routines for the test data, and supported the lab work. We appreciate the assistance in the lab and the test field by R. Graff, M. Graff, and H. Blanke. Open Access funding enabled and organized by Projekt DEAL.

Conflict of Interests

The authors declare no conflict of interest.

Data Availability Statement

The data that support the findings of this study are openly available in RWTH publication server at https://doi.org/10.18154/RWTH-2023-10931, reference number 202310931.

Keywords: Lithium-Ion Battery · Calendaric aging · Nickel-Rich · NCA · Silicon/Graphite · DVA · Capacity · Lifetime

[1] M. Dubarry, N. Qin, P. Brooker, *Curr. Opin. Electrochem.* **2018**, *9*, 106.
[2] J. D. McBrayer, M.-T. F. Rodrigues, M. C. Schulze, D. P. Abraham, C. A. Apblett, I. Bloom, G. M. Carroll, A. M. Colclasure, C. Fang, K. L. Harrison, G. Liu, S. D. Minteer, N. R. Neale, G. M. Veith, C. S. Johnson, J. T. Vaughey, A. K. Burrell, B. Cunningham, *Nat. Energy* **2021**, *6*, 866.
[3] J. E. Harlow, X. Ma, J. Li, E. Logan, Y. Liu, N. Zhang, L. Ma, S. L. Glazier, M. M. E. Cormier, M. Genovese, S. Buteau, A. Cameron, J. E. Stark, J. R. Dahn, *J. Electrochem. Soc.* **2019**, *166*, A3031.
[4] P. Keil, S. F. Schuster, J. Wilhelm, J. Travi, A. Hauser, R. C. Karl, A. Jossen, *J. Electrochem. Soc.* **2016**, *163*, A1872.

[5] F. Single, A. Latz, B. Horstmann, *ChemSusChem* **2018**, *11*, 1950.
[6] J. Schmitt, A. Maheshwari, M. Heck, S. Lux, M. Vetter, *J. Power Sources* **2017**, *353*, 183.
[7] P. Kuntz, O. Raccurt, P. Azaïs, K. Richter, T. Waldmann, M. Wohlfahrt-Mehrens, M. Bardet, A. Buzlukov, S. Genies, *Batteries* **2021**, *7*, 48.
[8] D. Werner, S. Paarmann, T. Wetzel, *Batteries* **2021**, *7*, 28.
[9] A. Krupp, R. Beckmann, T. Diekmann, E. Ferg, F. Schuldt, C. Agert, *J. Energy Storage* **2022**, *45*, 103506.
[10] I. Zilberman, S. Ludwig, A. Jossen, *J. Energy Storage* **2019**, *26*, 100900.
[11] I. Zilberman, J. Sturm, A. Jossen, *J. Power Sources* **2019**, *425*, 217.
[12] K. Kalaga, M.-T. F. Rodrigues, S. E. Trask, I. A. Shkrob, D. P. Abraham, *Electrochim. Acta* **2018**, *280*, 221.
[13] A. Zülke, Y. Li, P. Keil, R. Burrell, S. Belaisch, M. Nagarathinam, M. P. Mercer, H. E. Hoster, *Batteries & Supercaps* **2021**, *4*, 934.
[14] F. Hildenbrand, D. Ditscheid, E. Barbers, D. U. Sauer, *Appl. Energy* **2023**, *332*, 120395.
[15] P. Keil, A. Jossen, *J. Electrochem. Soc.* **2016**, *164*, A6066.
[16] Y. Yin, E. Arca, L. Wang, G. Yang, M. Schnabel, L. Cao, C. Xiao, H. Zhou, P. Liu, J. Nanda, G. Teeter, B. Eichhorn, K. Xu, A. Burrell, C. Ban, *ACS Appl. Mater. Interfaces* **2020**, *12*, 26593.
[17] G. M. Veith, M. Doucet, J. K. Baldwin, R. L. Sacci, T. M. Fears, Y. Wang, J. F. Browning, *J. Phys. Chem. C* **2015**, *119*, 20339.
[18] W. Lu, L. Zhang, Y. Qin, A. Jansen, *J. Electrochem. Soc.* **2018**, *165*, A2179.
[19] G. M. Veith, M. Doucet, R. L. Sacci, B. Vacaliuc, J. K. Baldwin, J. F. Browning, *Sci. Rep.* **2017**, *7*.
[20] I. Hasa, A. M. Haregewoin, L. Zhang, W.-Y. Tsai, J. Guo, G. M. Veith, P. N. Ross, R. Kostecki, *ACS Appl. Mater. Interfaces* **2020**, *12*, 40879.
[21] C. Stetson, Y. Yin, C.-S. Jiang, S. C. DeCaluwe, M. Al-Jassim, N. R. Neale, C. Ban, A. Burrell, *ACS Energy Lett.* **2019**, *4*, 2770.
[22] R. Jung, M. Metzger, D. Haering, S. Solchenbach, C. Marino, N. Tsiouvaras, C. Stinner, H. A. Gasteiger, *J. Electrochem. Soc.* **2016**, *163*, A1705.
[23] J. Bareño, I. A. Shkrob, J. A. Gilbert, M. Klett, D. P. Abraham, *J. Phys. Chem. C* **2017**, *121*, 20640.
[24] H. Liu, M. Wolfman, K. Karki, Y.-S. Yu, E. A. Stach, J. Cabana, K. W. Chapman, P. J. Chupas, *Nano Lett.* **2017**, *17*, 3452.
[25] S. Sallis, N. Pereira, P. Mukherjee, N. F. Quackenbush, N. Faenza, C. Schlueter, T.-L. Lee, W. L. Yang, F. Cosandey, G. G. Amatucci, L. F. J. Piper, *Appl. Phys. Lett.* **2016**, *108*, 263902.
[26] H. Hyun, H. Yoon, S. Choi, J. Kim, S. Y. Kim, T. Regier, Z. Arthur, S. Kim, J. Lim, *Energy Environ. Sci.* **2023**, *16*, 3968.
[27] C. Xu, K. Märker, J. Lee, A. Mahadevegowda, P. J. Reeves, S. J. Day, M. F. Groh, S. P. Emge, C. Ducati, B. Layla Mehdi, C. C. Tang, C. P. Grey, *Nat. Mater.* **2020**, *20*, 84.
[28] M.-T. F. Rodrigues, K. Kalaga, S. E. Trask, I. A. Shkrob, D. P. Abraham, *J. Electrochem. Soc.* **2018**, *165*, A1697.
[29] L. K. Willenberg, *Volume expansion and its effects on the ageing of a cylindrical lithium-ion battery*, Ph.D. thesis, Rheinisch-Westfälische Technische Hochschule Aachen **2020**.
[30] S. Klick, G. Stahl, D. U. Sauer, *Energy Technol.* **2023**, *12*.
[31] M. Lewerenz, G. Fuchs, L. Becker, D. U. Sauer, *J. Energy Storage* **2018**, *18*, 149.
[32] M. E. Wojtala, F. B. Planella, A. A. Zulke, H. E. Hoster, D. A. Howey, Investigating changes in transport, kinetics and heat generation over NCA/Gr-SiOx battery lifetime, in *2022 IEEE Vehicle Power and Propulsion Conference (VPPC)* **2022** pages 1–6.
[33] M. E. Wojtala, A. A. Zülke, R. Burrell, M. Nagarathinam, G. Li, H. E. Hoster, D. A. Howey, M. P. Mercer, *J. Electrochem. Soc.* **2022**, *169*, 100527.
[34] Y. Wu, X. Liu, L. Wang, X. Feng, D. Ren, Y. Li, X. Rui, Y. Wang, X. Han, G.-L. Xu, H. Wang, L. Lu, X. He, K. Amine, M. Ouyang, *Energy Storage Mater.* **2021**, *37*, 77.
[35] X. H. Liu, J. W. Wang, S. Huang, F. Fan, X. Huang, Y. Liu, S. Krylyuk, J. Yoo, S. A. Dayeh, A. V. Davydov, S. X. Mao, S. T. Picraux, S. Zhang, J. Li, T. Zhu, J. Y. Huang, *Nat. Nanotechnol.* **2012**, *7*, 749.
[36] J. Vetter, P. Novák, M. Wagner, C. Veit, K.-C. Möller, J. Besenhard, M. Winter, M. Wohlfahrt-Mehrens, C. Vogler, A. Hammouche, *J. Power Sources* **2005**, *147*, 269.
[37] E. Peled, S. Menkin, *J. Electrochem. Soc.* **2017**, *164*, A1703.

Manuscript received: February 8, 2024
Revised manuscript received: March 4, 2024
Version of record online: April 9, 2024